Catalysis Letters (2021) 151:1142–1154
https://doi.org/10.1007/s10562-020-03348-z

Computational Study of Transition-Metal Substitutions in Rutile TiO_2 (110) for Photoelectrocatalytic Ammonia Synthesis

Benjamin M. Comer[1] · Max H. Lenk[2] · Aradhya P. Rajanala[3] · Emma L. Flynn[4] · Andrew J. Medford[1]

Received: 19 March 2020 / Accepted: 31 July 2020 / Published online: 25 August 2020

Abstract

Synthesis of ammonia through photo- and electrocatalysis is a rapidly growing field. Titania-based catalysts are widely reported for photocatalytic ammonia synthesis and have also been suggested as electrocatalysts. The addition of transition-metal dopants is one strategy for improving the performance of titania- based catalysts. In this work, we screen *d*-block transition- metal dopants for surface site stability and evaluate trends in their performance as the active site for the reduction of nitrogen to ammonia on TiO_2. We find a linear relationship between the *d*-band center and metal substitution energy of the dopant site, while the binding energies of N_2, N_2H, and NH_2 all are strongly correlated with the cohesive energies of the dopant metals. The activity of the metal-doped systems shows a volcano type relationship with the NH_2 and N_2H energies as descriptors. Some metals such as Co, Mo, and V are predicted to slightly improve photo- and electrocatalytic performance, but most metals inhibit the ammonia synthesis reaction. The results provide insight into the role of transition-metal dopants for promoting ammonia synthesis, and the trends are based on unexpected electronic structure factors that may have broader implications for single-atom catalysis and doped oxides.

Graphic Abstract

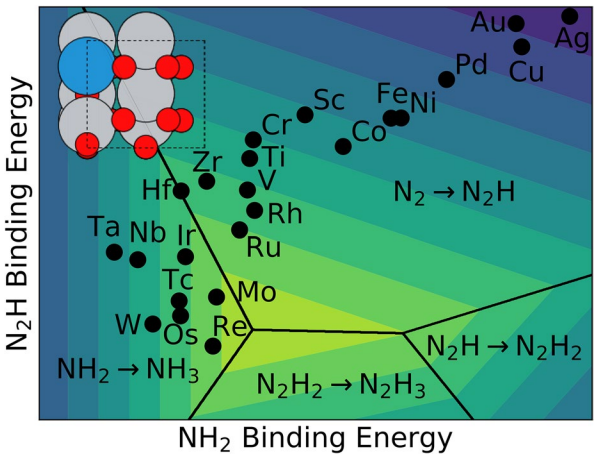

Keywords Nitrogen fixation · Single atom catalysis · Density functional theory

1 Introduction

The fixation of atmospheric nitrogen has long been one of the prime challenges in chemistry and chemical engineering [1, 2]. The Haber–Bosch process has been the route of choice for performing nitrogen fixation for the past century,

Benjamin M. Comer and Max H. Lenk have contributed equally to this work.

Electronic supplementary material The online version of this article (https://doi.org/10.1007/s10562-020-03348-z) contains supplementary material, which is available to authorized users.

Extended author information available on the last page of the article

permitting much of the population growth over that period [3]. However, this process has significant drawbacks, including high CO_2 emissions and centralized production due to large capital requirements [4]. The Haber–Bosch process's considerable contribution to CO_2 emissions has been an increasingly pressing concern for the global community, as it accounts for 340 million tonnes of CO_2—fully 2% of the carbon emissions worldwide [5, 6]. For this reason, supplanting the Haber–Bosch process would represent a significant contribution to global efforts to curb climate change.

Due to the various drawbacks of the Haber–Bosch process, researchers have sought alternative means of producing fixed nitrogen [4, 7–11]. Two strategies that have received significant recent interest are electrocatalysis [7] and photocatalysis [12]. However, making either of these technologies viable presents a significant challenge. Electrochemical nitrogen fixation requires generating electricity and transporting electrons to the catalyst surface to perform the reaction [9]. The need for both solar and electrocatalytic cells may limit the viability of electrochemical processes in the developing world. An alternative route is photochemical nitrogen fixation, where the catalyst is placed in direct contact with sunlight, air, and water vapor to produce fixed nitrogen. The photochemical route has the potential to operate with low capital investment and simpler infrastructure, making it promising for low-resource environments [4].

The scientific community has known of photochemical nitrogen fixation for decades, but inconsistent results, questions of contamination, and low rates have discouraged further study [12, 13]. Dhar was the first to investigate photocatalytic nitrogen [14], and the first well-controlled experiments were performed decades later when Schrauzer and Guth independently re-discovered the process [15]. Schrauzer and Guth were able to establish the production of NH_3 in sterilized desert sands under illumination [15], including confirmation via isotopic labeling [16]. Numerous independent experiments have been performed over the years and reported photochemical production of NH_3 over titania materials [17–22], though legitimate skepticism has remained due to issues with contamination [13, 23, 24], interference [25, 26], and inconsistent results [12]. However, recent experiments utilizing ambient pressure X-ray photoelectron spectroscopy have observed reduced nitrogen compounds only under illumination [27]. These experiments provide direct experimental evidence that photoinduced nitrogen reduction occurs on titania surfaces, though the presence of carbon-based impurities was found to be a critical enabler of the process.

One route to increasing reaction rates is the inclusion of transition-metal dopants in TiO_2 [28]. Transition-metal dopants can increase rates via at least two distinct mechanisms: increasing the amount of photogenerated electrons that reach the surface by improving absorption and charge separation, or by altering the kinetics of the surface reaction. Transition-metal doping has been previously explored to improve the performance of TiO_2 photocatalysts [29–31]. In particular, early work on photocatalytic nitrogen fixation tested a variety of metal dopants. These studies found that several noble metals [32] and iron in particular increase yields [15, 16, 18, 19, 32, 33]. In these studies the dopant metals were co-precipitated with the TiO_2 samples, thus having significant concentrations in the bulk. These studies were also performed without the use of isotopic labeling, and careful controls are not always included, making interpretation difficult. More recently, Hirakawa et al. used a modern photochemical setup along with isotopic labeling and found that depositing noble metals (Ru, Pt, Pd) onto an already prepared rutile (110) surface led to a decrease in reaction rates [22]. This decrease in rates, along with detailed experimental and theoretical studies on the role of iron dopants [19, 34] suggests that the primary mechanism of these previously-reported dopants is enhanced charge separation. However, transition-metal dopants are also known to affect the surface properties in a range of other materials and reactions [34–40]. In particular, the field of "single-atom catalysis" has revealed that isolated transition-metal sites supported on oxide materials can exhibit remarkable catalytic properties [41–43]. Yet, relatively little effort has focused on understanding how isolated transition-metal atom dopants affect the surface reactivity of oxides for the conversion of nitrogen to ammonia [44–48].

In this work, we focus on the potential of isolated transition-metal atoms substituted into the rutile (110) titania surface (see Fig. 1) as a potential route to improve the surface kinetics of the nitrogen reduction reaction. We screen the *d*-block transition-metals substituted into the (110) surface in two different configurations corresponding to formal oxidation states of 2+ and 4+. We analyze the trends present across the periodic table for the dopant metal substitution energy, N_2, N_2H, and NH_2 adsorption energy. We also map out the thermodynamics of all N_2 reduction pathways and use this to assess the most favorable reaction mechanism. Finally, we assess the expected improvement in reaction rates from forming metal dopant sites on the surface. In this analysis, we consider both electrocatalytic and photocatalytic N_2 reduction. The results illustrate that there are clear correlations in the metal substitution and adsorption energies with the *d*-band center and cohesive energies, respectively. We also find scaling relations between the surface species. These scaling relations result in an optimum in the rate-limiting potential for nitrogen reduction as a function of N_2H and NH_2 adsorption energies.

2 Results and Discussion

Rutile TiO_2 (110) is chosen as a model surface based on the experimentally observed correlation between rutile content and reaction rates for photocatalytic nitrogen fixation [15]. Additionally, there is a rich literature on the surface science of rutile (110) [49–52], and recent surface-science experiments and DFT calculations indicate that carbon substitution defects on the rutile (110) surface are active for photocatalytic nitrogen reduction [27]. From this model surface, slabs containing metal dopants at the surface formally in the 2+ and 4+ oxidation states are generated for each dopant metal. These oxidation states may not represent the true oxidation state of each site, but rather represent the oxidation state the site would take on if all Ti metal atoms retained the 4+ oxidation state. We also note that these models are similar to those studied previously in the literature [39, 53]. In total, all d-block transition-metals, except Mn (24 total), are screened for their surface metal substitution energy and activity for nitrogen reduction. The binding energies of N_2H and NH_2 have been identified as descriptors for activity in the literature as they are typically involved in the rate-limiting steps [34, 54, 55]. Thus, these energies have been calculated to assess the activity of generated surfaces. Full details of the calculation methodology are in the Sect. 4.

2.1 Trends in Active Site Metal Substitution Energies

The stability of substituted metal surface sites is examined with respect to the position of their *d*-band center. In Fig. 2a, the metal substitution energy of the studied active sites has been plotted against the location of the *d*-band center of the corresponding transition-metal see Eq. 2. The pure metallic form is the reference for the metal substitution energy of each metal substituted site. The *d*-band centers are calculated from the metallic bulk state rather than the single atom [56].

The plot indicates there is a strong correlation between the *d*-band center and metal substitution energy of the metal substitution ($R^2 = 0.91$ and 0.79 for 4+ and 2+ respectively).

The correlation between the *d*-band center, a bulk metal property, and the stability of isolated metal atoms is somewhat surprising. However, the stability of the bulk metal also plays a role in determining the stability of the isolated site, which may explain some correlation, although the *d*-band center was found to be a better descriptor than the cohesive energy. The observed trends are also consistent with the observation that the interaction between metal surfaces and oxygen weakens from left to right on the periodic table, as predicted by the *d*-band model [57]. This trend implies that the metals most able to integrate into a surface are those with the most favorable interaction with oxygen. A similar relationship has been reported previously for doped rutile oxides [58] and oxide-supported single-atom catalysts [43]. Other reports suggest that the electronegativity of the substituted metal is the relevant descriptor predicting stability [39]. The electronegativity is also correlated with the metal substitution energy ($R^2 = 0.81$ and 0.62 for 2+ and 4+ respectively,

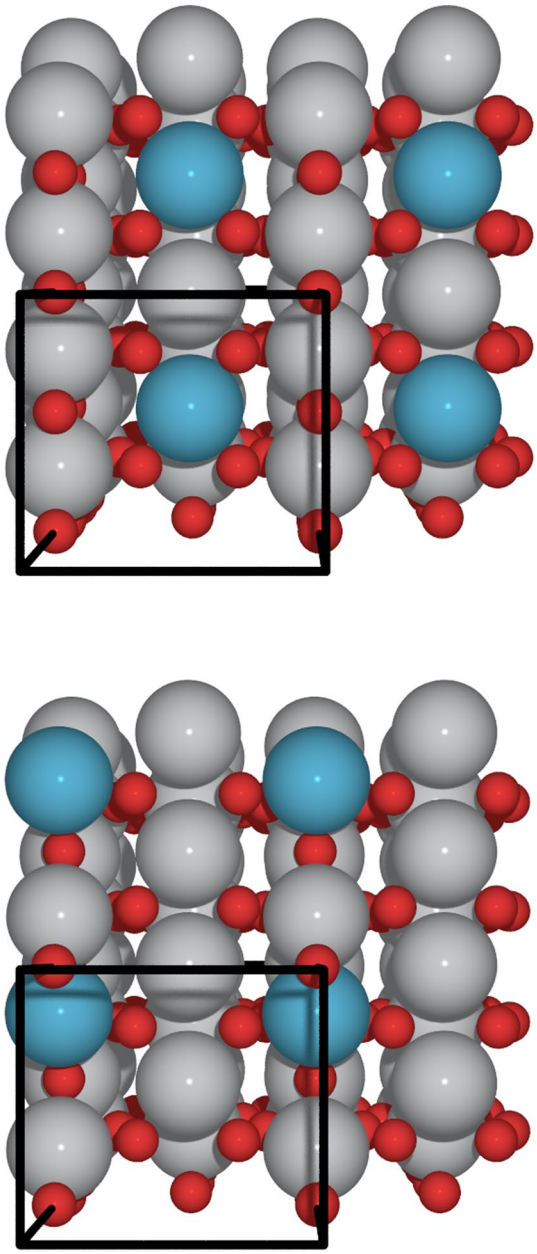

Fig. 1 An example of the screened 2+ (top) and 4+ (bottom) slabs. For 2+ sites the substituent metal has replaced a sixfold Ti atom (seen in blue) and a bridging oxygen vacancy has been formed to allow the metal to enter the 2+ oxidation state. For 4+ sites the substituent metal has replaced a fivefold Ti atom (seen in blue) resulting in a 4+ formal oxidation state

see Fig. S3), but not as strongly as the *d*-band center of the metal ($R^2 = 0.79$ and 0.91, see Fig. 2). The fact that both of these quantities correlate with the metal substitution energy is not surprising, as a lower energy *d*-center indicates a more favorable addition of electrons, which is similar to the concept of electronegativity. The main exceptions to this trend are Ti, Zr, Hf, and Ag. The first three can be rationalized easily since all three lie in the same column of the periodic table, which is the same as the host metal, Ti. The improved stability of substituent metals within the group lines up with the chemical intuition since these elements have the same number of valence *d* electrons. This chemical similarity affords approximately 1.5 eV of improved stability relative to the trend. The final outlier, Ag, is more difficult to explain. However, the *d*-band center of Ag is itself an outlier for its position on the periodic table. This deviation may indicate that more complex bonding interactions are involved.

These results have implications for the relative stability of single-atom sites over surface metal clusters or bulk substitutions in TiO_2, and will relate to the feasibility of synthesizing metal-doped surfaces experimentally. We note that many of the metal substitution energies are exceedingly high (up to 10 eV) indicating that many of these surface sites are unlikely to be experimentally feasible. Some elements (Y, Sc, Zr, Hf) favor integration into the surface structure rather than the formation of surface metal clusters (see Tables S1 and S2). Conversely, noble metals such as Rh and Pt do not integrate into the surface favorably and will tend to form surface nano-clusters. This result agrees with TEM measurements in the experimental literature, indicating that clusters of metals such as platinum, silver, gold, nickel, rhodium form on a TiO_2 surface [59–62] and rutile's reputation as a support [63]. A metal's ability to form surface sites is also dependent on the relative stability of bulk substitution, since a dopant that is more stable in the bulk than the surface will tend to segregate into the bulk rather than forming surface sites. Figure 2b shows that the 4+ surface sites are more stable than the bulk substitutions for all metals studied. The stability of surface sites relative to bulk integration suggests that bulk synthesis techniques such as co-precipitation should lead to a concentration of surface sites that exceeds the concentration of bulk sites for all metals considered. The correlation between the bulk metal substitution energies of dopant metals and their corresponding 4+ surface sites (Fig. 2b) is also striking, indicating that bulk and surface integration are controlled by similar electronic structure interactions.

Figure 2a also indicates that the oxidation state of the surface site that forms is dependent on the energy of the substituent metal's *d*-band center. Elements with more negative *d*-band centers tend to favor forming 2+ surface sites, whereas more positive *d*-band centers favor 4+ sites, with the cross-over point being approximately 0.8 eV below the Fermi-level. This trend makes intuitive sense, as a more negative *d*-band center implies that the addition of electrons is more favorable, making the more negative oxidation state more stable. For most metals studied, the 2+ site is either more stable or nearly as stable, suggesting that the 2+ substitutions are generally more favorable. An alternative interpretation is that the inclusion of metal dopants favors the formation of surface oxygen vacancies, since the 2+ site involves an oxygen vacancy. The reactivity of oxygen vacancies is typically greater than the pristine surface, so promoting oxygen vacancy formation may be yet another indirect mechanism through which metal dopants affect catalytic activity.

2.2 Trends in Nitrogen Adsorption and Cohesive Energies

The adsorption of the inert N_2 molecule is required for nitrogen fixation, and the first hydrogenation to N_2H is known to be the potential-limiting step on pure TiO_2 [34]. In addition, the $NH_2 \rightarrow NH_3$ reaction has been identified as potential limiting on some materials [54]. This suggests that the trends in N_2, N_2H, and NH_2 binding will provide an indication of a metal's ability to promote nitrogen reduction. The N_2 and N_2H energies are calculated for both 2+ and 4+ slabs to screen the surface's ability to reduce N_2. The N_2H binding energy is > 1.5 eV for all 4+ sites (see Table S2), therefore the subsequent analysis focuses exclusively on 2+ sites.

The results for N_2, N_2H, and NH_2 adsorption on 2+ sites as a function of periodic table group are shown in Fig. 3. The results differ from the typical linear correlation that we expect from the *d*-band model [64], and instead, show relatively quadratic behavior with a maximum near the middle of the *d*-block at Os and Re for N_2 and N_2H respectively. Similar results are found for NH_2 adsorption (Fig. 3c), though the magnitude of the adsorption energy varies, and there is small upward trend near the middle of the *d*-block.

While the N_2, N_2H, and NH_2 binding observed deviates from the near-linear correlation expected from the *d*-band model, we find a linear correlation between the binding energies and the *d*-band contributions of the cohesive energies of the corresponding bulk systems (Fig. 4) although the correlation is relatively weak in the case of N_2. Cohesive energy is defined as the change in energy associated with isolated, neutrally charged atoms being brought together to form a bulk material [65]. A metal's cohesive energy is made up of a *d* contribution and a *s* contribution. Cohesive energies have generally been a measure of the "bulk-nobleness" of a metal [66], with higher cohesive energies correlating to a more noble character. The metals with the highest "bulk-nobleness" are in the center of the *d*-block and resist corrosion due to the difficulty of breaking their strong metal–metal bonds. In our case, the inverse is true: the stronger the metal–metal

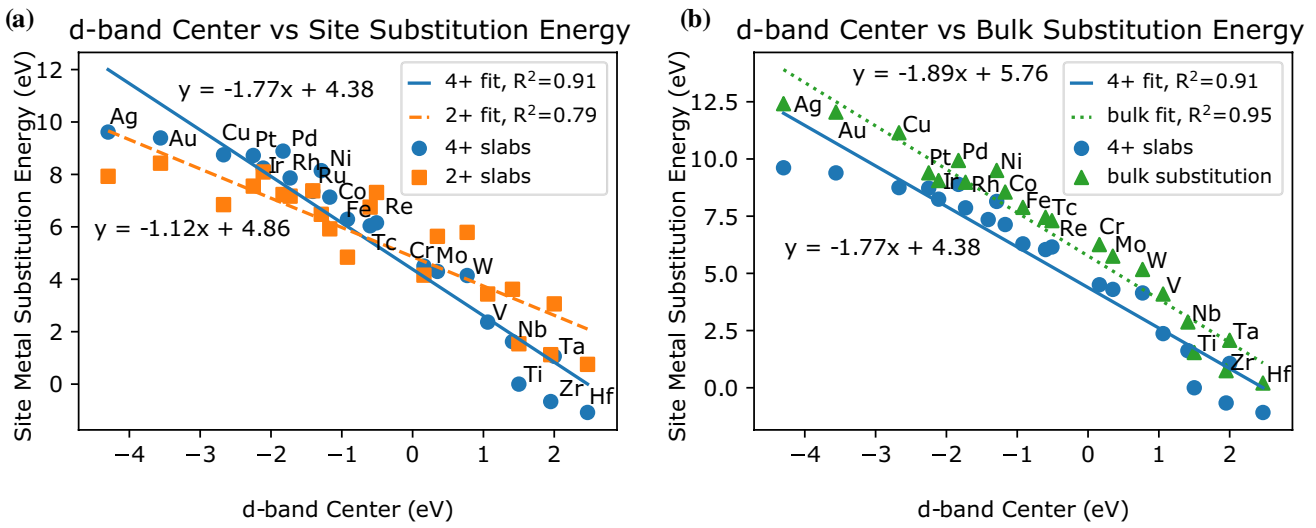

Fig. 2 **a** The metal substitution energy see Eq. 2 of 4+ surface sites (blue) and 2+ surface sites (orange) with respect to their bulk metallic state vs. the metallic *d*-band center. **b** The metal substitution energy of 4+ surface sites (blue) and bulk substitutions (green) with respect to their bulk metallic state vs. the metallic *d*-band center. *d*-band centers were obtained from [56]. Only metals whose *d*-band center was previously reported in [56] are included

bonds of the bulk material, the stronger the interaction between the metal and a given nitrogen species.

The correlation between *d*-band contribution to cohesive energy and binding is the strongest for N_2H and NH_2 (Fig. 4b, c). These two species show a relatively strong quadratic dependence (Fig. 3b, c) suggesting that the bonding of nitrogen species to these substituent metals is similar to that of forming metal–metal bonds of the original bulk material. Thus, we hypothesize that the physics of nitrogen bonding to these substituent sites is similar to the bonding between single metal atoms and a bulk metal. A similar quadratic trend is seen for N_2 adsorption in Fig. 4a, though there are several outliers near the middle of the *d*-block (Tc, Ru, Re, Os, Ir) that bind N_2 substantially stronger than predicted by the cohesive energy descriptor. The origin of this anomalously-high reactivity toward N_2 is not clear, though we note that the bonding mechanism changes between physisorption for early/late metals and chemisorption for more reactive metals, indicating that the quadratic trend may still hold for chemisorption.

The trends observed for site metal substitution energy (Fig. 2) and nitrogen compound adsorption energy (Fig. 4) differ qualitatively from trends observed in bulk metals. For single transition-metal dopant atoms, the *d*-band center controls metal substitution energy, while the cohesive energy controls adsorption energy. In bulk metals the inverse is true: the *d*-band center controls a material's ability to bind gas-phase species, whereas the cohesive energy controls how stable the material is [66]. This suggests that the origins of scaling relations for single-atom catalysts or dopant sites may differ from the case of bulk metals. However, the trend does not seem to hold in the case of 4+ sites (see Table S2), and prior work suggests that adsorption energy of oxygen on single metal atoms is correlated to the *d*-band center [57], so the trend is not general. The implication of different factors controlling the scaling relations of different adsorbates is that these adsorbates will also not scale with each other. This suggests that single metal atoms or dopants may be able to "break" the scaling relations between adsorbates and reach more active regions of the catalytic phase space [67, 68].

2.3 Trends in Catalytic Activity for Nitrogen Reduction

The photocatalytic activity of doped TiO_2 surfaces can be assessed by computing the maximum thermodynamic barrier with electrons at the conduction band edge potential [34], while the electrocatalytic activity of doped TiO_2 surfaces can be assessed by computing the thermodynamic limiting potential [39, 70]. The computational hydrogen electrode (CHE) provides a route to computing the thermochemical potential of electrons at the TiO_2 surface (Sect. 4.3), and the resulting analysis provides only a thermodynamic picture of the reaction pathway. This analysis establishes a lower bound on the kinetics and correlates well with experimental trends in the literature [71].

Computing the maximum barrier or limiting potential requires the free energies of each state along a given reaction pathway. The full thermodynamics of the N_2 reduction reaction pathways on all 2+ sites were calculated, allowing the

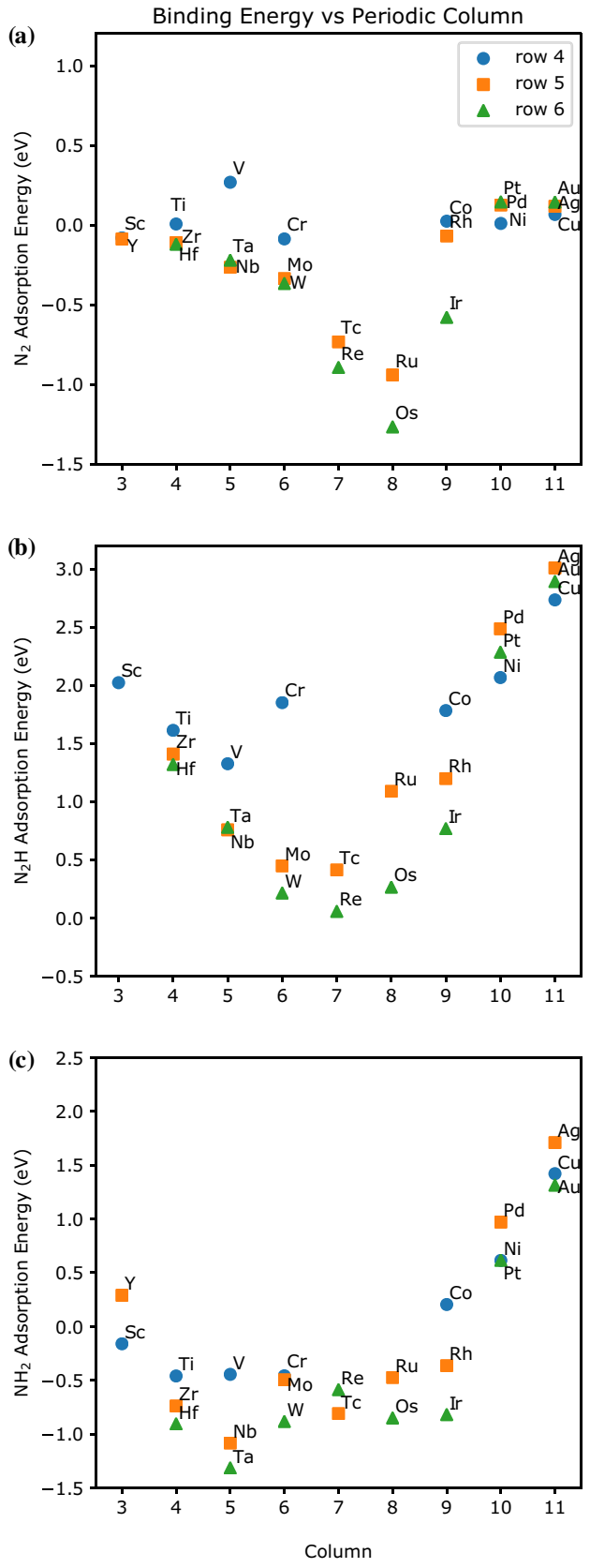

Fig. 3 The binding energies of (a) N_2, (b) N_2H and (c) NH_2 plotted against the periodic column for 2+ metal substituent sites

generation of free energy diagrams for all possible reaction pathways (Figs. S4–S109, Table S1). H¨oskuldsson et al. [54] also previously found strong scaling relations between the binding of nitrogen compounds and the N_2H binding energy for rutile metal oxides. The binding energies of all species are fit to linear scaling relations with N_2H and NH_2 as descriptors to assess the scaling relations for this system (Fig. S1). The scaling relations have a root mean squared error on the order of 0.2 eV (see Figures S1 and S2), consistent with general scaling relations for other reactions [72]. The N_2H and NH_2 were also used to fit scaling relationships for all electrochemical steps, yielding similar accuracy to scaling relations for individual species (Fig. S2). These scaling relations directly predicting reaction energies are used for subsequent analyses.

A primary consideration when assessing the electrocatalytic activity of a surface is the largest thermochemical barrier. Thermochemical steps do not involve electron transfers, so they are not considered when computing the limiting potential. However, they may still present a substantial barrier that will affect the overall rate. The largest thermochemical barriers for each surface can be seen in Table S4. The three steps with significant thermochemical barriers are N_2 adsorption, NH_2–NH_2 scission, and NH_3 desorption. For the case of the most promising dopant, Mo, the adsorption of N_2 is exergonic by − 0.27 eV, which is large enough to yield reasonable to N_2* coverages. However, competitive adsorption with H_2O and O_2 have not been considered. Moreover, there is a substantial thermochemical barrier of 0.83 eV for NH_3 desorption. Desorption of NH_3 is the thermochemical limiting step for most dopants, suggesting that NH_3 may exist at high coverages or even poison the surface. However, solvation effects have been neglected, and the free energy is computed at a chemical potential of NH_3 equivalent to 1 bar, suggesting that NH_3 desorption may not be limiting in aqueous solutions with low NH_3 concentrations. Some of the noble dopants (Pd, Ag, Au, and Cu) also show substantial thermochemical barriers of 0.5–1.5 eV for NH_2–NH_2 scission, indicating that rates for these metals will be low even at the limiting potential. A more detailed kinetic analysis of both electrochemical and thermochemical activation energies is required to predict the electrocatalytic rate for any dopant, but this thermochemical analysis provides lower bound for the kinetic barrier.

We assess the ability of dopant metals to improve photocatalytic nitrogen reduction. This is calculated based on the largest thermodynamic barrier at a reductive potential equal to the conduction band edge of TiO_2 (approximately − 0.15 V vs. RHE [73]). This approach assumes that the conduction band edge of TiO_2 is not significantly affected by the presence of the dopant, and neglects improvements in other photochemical properties such as introduction of defect levels, charge separation or carrier lifetime.

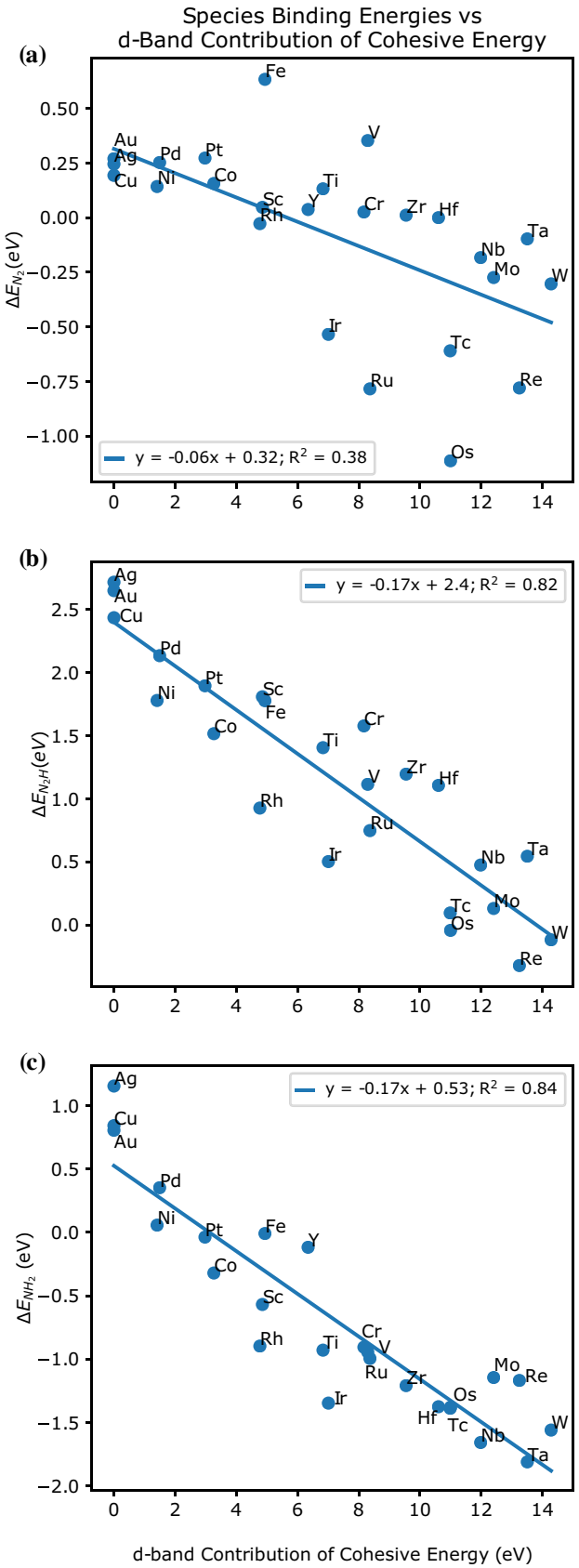

Fig. 4 The *d*-band contribution to cohesive energies vs. the binding energies of **a** N_2, **b** N_2H, **c** NH_2 for 2+ metal substituent sites. The *d*-band cohesive energy contributions obtained from Turchanin and Agraval [69]

Nonetheless, it provides a good starting point for assessing the impact of dopant metals on the surface catalytic properties. The highest thermodynamic barrier for the best reaction pathway is plotted vs. the NH_2* binding energy in Fig. 5. The results are qualitatively similar to the electrochemical limiting potentials in Fig. 6, but there are some deviations that occur for two reasons. The first is that the photochemical analysis includes both thermochemical and electrochemical steps. The desorption of NH_3* is a thermochemical step that becomes rate-limiting for reactive surfaces. For less reactive surfaces the electrochemical step of N_2 hydrogenation is rate-limiting, which becomes slightly more favorable under the applied bias, effectively shifting the right side of the volcano downward. The second reason for deviation is that multi-electron transfers are less sensitive to small potentials, so dopants such as Re which have relatively unstable $N_2H_{x>2}$ states are not as favorable under photocatalytic conditions. Overall, the results suggest that the minimum thermodynamic barriers of 1.06 eV, 0.97 eV, 0.96 eV, 0.90 eV, 0.82 eV, for Mo, V, Hf, Ir, and Rh, respectively. This represents a substantial improvement over the 1.26 eV limiting potential for pure Ti, indicating that these metals may act as surface promoters for photocatalytic nitrogen reduction if kinetic barriers are low.

The electrochemical limiting potential is calculated for all surfaces to assess their ability to reduce N_2 under applied bias. The results are plotted against the NH_2 binding energy in Fig. 6a. This plot reveals a clear volcano relationship between the NH_2 binding energy and the limiting potential. In contrast to prior work by H¨oskuldsson et al. [54] and Montoya et al. [55], we find that the NH_2 binding energy is a slightly more reliable descriptor than N_2H binding; however these quantities are linked by scaling relations, indicating that either descriptor will provide consistent trends. In this case, the limiting step shifts from NH_2 desorption on the left to N_2 hydrogenation on the right, with most dopants being limited by NH_2 desorption. This means that NH_2 adsorption energy directly controls the reactive side of the volcano, and explains why it is an accurate descriptor in this case.

To better understand the relationship between the descriptors, limiting potential, and limiting steps, the fits of the scaling relations (see Fig. S2) were used to generate a two dimensional volcano plot (Fig. 6b).We note that the points on this plot are filled in with their calculated limiting potential from DFT, but placed based on their predicted limiting potential from the scaling relations, enabling direct assessment of the error due to scaling relations. As with the scaling relations, the root mean squared error of the predicted

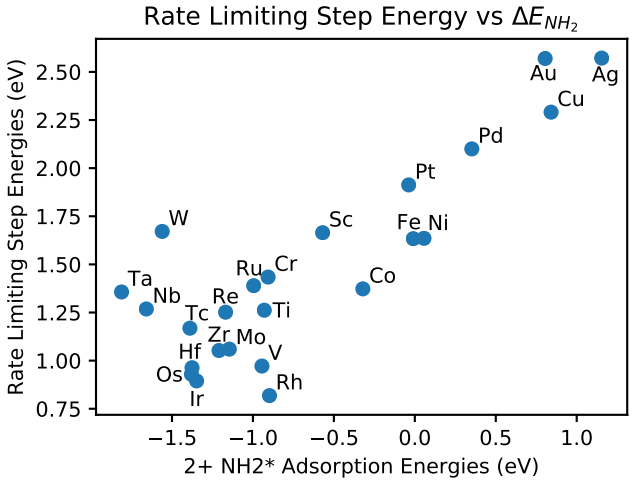

Fig. 5 The highest barrier observed vs the NH_2 binding energy with the potential set to band edge of rutile. The data for this plot can be seen in Table S5. Any surface for which a full path was not available has been excluded

limiting potential in Fig. 6b is roughly 0.2 V. The results confirm the findings from Fig. 6a, but provide additional insight into the limiting steps. The results also show that the optimal limiting potential is still relatively large (~ − 0.8 V), and that Mo is near-optimal. There are also a few dopants that deviate from the trend. Notably, Os, Ir, and Hf are on the reactive side of the volcano, but the potential limiting step is N_2H formation [34, 54]. Nonetheless, these elements fortuitously fall close to the trend predicted by the volcano plot.

Overall, the results suggest that several dopants are capable of improving the performance over pure TiO_2. The elements that show significant improvement are Mo, Rh, and Re. Mo is relatively inexpensive and abundant, whereas Re and Rh are relatively scarce [74]. Moreover, synthesis may be a challenge since the metal substitution energy of the surface sites is generally positive relative to the bulk metals (Fig. 2). Nonetheless, the results indicate that Mo is the most promising dopant for reducing the thermodynamic limiting potential of ammonia synthesis on TiO_2. This is also interesting since Mo is known to play a role in biological nitrogen fixation [75], and Mo-based transition-metal complexes are known to reduce nitrogen in homogeneous catalysis [76]. We also note that for metals that are not predicted to improve the rate of reaction relative to Ti the observed reaction rates would appear very similar to the rate of pure Ti, as Ti sites would dominate observed turnovers. Thus, suppression of rates observed experimentally is likely related to other effects such as reduced charge generation/transport in the bulk and near-surface region.

Experimental observations can provide further insight into the computational predictions. Several prior reports have investigated transition-metal dopants for enhancing photocatalytic ammonia production on TiO_2 [15, 22, 32]. Interestingly, Schrauzer et al. report increases in ammonia yield in the presence of Mo dopants [15], though this report comes from the early literature and rigorous controls [77] or isotopic labeling studies [78] were not included. Moreover, the same report revealed enhanced rates for Fe and Ni, so the confirmation of the prediction regarding the former two should be treated with caution. The rate enhancement for noble metals such as Ru, Rh, and Pd is conflicting even in the early literature, with Schrauzer and Guth reporting no enhancement [15]. However, Ranjit et al. reported enhancement for all noble metals with the most significant improvement for Ru [32]. In all of these systems, the metal dopants were incorporated via coprecipitation, and catalysts were polycrystalline TiO_2, indicating that the metals may also enhance yields via charge separation, mediation of crystallization, or other mechanisms [12]. Hirakawa et al. added Ru, Pt, and Pd to pre-synthesized TiO_2 particles and reported no significant improvement in the reaction rates [22]. These experiments are more consistent with the computational model system used in this study since only surface properties are affected, and the results are consistent with the prediction that these noble metals will not improve the rate. However, further systematic and well-controlled experiments that characterize the state of the metal incorporation in the TiO_2 surface are required to validate the predicted trends.

3 Conclusions

The stability of metal dopant surface sites and their effects on the reaction thermodynamics of N_2 reduction on rutile (110) are studied using DFT. We find that the metal substitution energy of these doped surface states is strongly related to the location of the *d*-band center of the substituted metal, with a trend consistent with the *d*-band model. We also find a correlation between the cohesive energy of metals and their N_2H and NH_2 binding energy on the surface, suggesting that the bonding of nitrogen species is similar to that of bulk metals. Finally, we investigate the effects of dopant sites on the full reaction pathways for 2+ sites on all studied metals. We find a clear volcano relationship between NH_2 binding and both the electrochemical limiting potential and the highest thermodynamic barrier for photocatalytic reactions. The formation of Rh 2+ sites is proposed to yield a slight improvement of reaction rates in both electrocatalysis and photocatalysis. Other metals commonly used in catalysis, such as Pt and Pd are predicted to have a limited or detrimental effect on the surface catalytic properties of TiO_2 for nitrogen reduction. This suggests that the role of metal dopants in photocatalytic ammonia synthesis by TiO_2 is likely related to modifications of bulk properties in most cases. However, the existence of clear trends in the

metal substitution energy and reactivity of single metal atom dopants toward nitrogen intermediates suggests that computational design of metal-doped oxide materials is a promising strategy for other oxide systems and/or other nitrogen conversion reactions.

4 Methods

4.1 Density Functional Theory Calculations

All first principles calculations are performed in the Quantum Espresso software package [79]. The TiO_2 slabs and atomistic images are created using the Atomic Simulation Environment (ASE) package [80]. Spin polarization is used in all simulations to ensure the lowest energy spin state is obtained for each site. The BEEF-vdW functional [81] is used with plane wave cutoff of 550 eV and a Monkhorst–Pack k-point grid spacing of $4 \times 4 \times 1$ [82]. The efficiency versions of the standard solid state psuedopotentials [83] (SSSP) are used for all calculations because of their high reported accuracy [84]. The convergence threshold is set at 10^{-6} eV and Fermi- Dirac smearing of 0.1 eV is used. All structures are converged to a maximum force smaller than 0.05 eV/A using the BFGS line search algorithm. Adsorption energies are obtained from the DFT calculations by subtracting the energy of a clean slab and the energy of the free gas molecule from the energy of the gas adsorbed to the slab:

$$E_{adsorption} = E_{slab+adsorbate} - E_{slab} - E_{adsorbate} \tag{1}$$

For all calculations the magnetic moments have been perturbed. Most elements the magnetic moments were perturbed near zero. However, for elements known to show complex magnetic states (Ni, Fe, Co, Cr) the magnetic moments have been initialized to the natural magnetic moment of these elements in the bulk metal form. All obtained magnetic moments for the unit cells may be seen in Table S6. It should be noted that non-integer values were obtained for several spin states, which is likely a result of the GGA approximation.

Previous literature suggests that Hubbard + U corrections are needed to properly capture the behaviour of d-electrons within DFT [85]. However, we have chosen not to include these corrections in this work. This was done to avoid issues created by selecting + U values for all metals, for which there is no accepted universal method [53, 58]. Additionally, the primary concern of this work is capturing trends in the surface adsorption properties, which may change with the addition of + U corrections. However, previous work has been performed on rutile oxides [58] and doped rutile TiO_2 [53], finding that the trends observed with the addition of + U corrections are preserved by GGA for those systems for oxygen evolution reactions.

4.2 Thermochemistry

To calculate the adsorption energy at standard temperature and pressure, the thermochemistry package from ASE is used [80]. The contributions of zero point energy (ZPE) have been included for all systems. Free gasses are approximated in the ideal gas limit, and adsorbed gasses in the harmonic limit [86]. A frequency cutoff of 33 cm^{-1} for low frequency modes was selected. The vibrational mode for all metals were assumed to be approximately the same as those of the respective species adsorbed to the oxygen vacant TiO_2 (110) surface, thus the same thermodynamic correction values are applied to all species of the same type.

Site metal substitution energies were calculated based on the energy of displacing the metal dopant atom from it's bulk metallic form into the position of a titanium atom, and placing the titanium atom into a bulk metallic titanium form. The following formula was used:

$$\Delta E_s = E_{Ti_{n-1}O_yM} + E_{Ti_{(m)}} - E_{M_{(m)}} - E_{Ti_nO_y} \tag{2}$$

where ΔE_s is the metal substitution energy of the dopant metal site, $E_{T\,in-1}O_y\,M$ is the energy of the doped surface, $E_{T\,i(m)}$ is the per atom energy of bulk Ti, $E_{M(m)}$ is the per atom energy of the dopant metal, and $E_{T\,in}O_y$ is the energy of the undoped surface.

4.3 Photochemistry

The photochemistry has been treated using the methods outlined by Hellman et al. [87]. Within this framework, the effects of excited states are neglected allowing the treatment of excited electrons and holes using the computational hydrogen electrode model (CHE). In this formalism, the reference electrode is set by setting the free energy of hydrogen evolution reaction (HER) to zero:

$$H^+ + e^- \rightarrow H_2; \quad \Delta G = 0 \;\; at \;\; U = 0 \tag{3}$$

The potentials of electrons and holes are set at the value of the band edges of the rutile [73].

4.4 Model Surface Generation

The surfaces are constructed with 4 TiO_2 tri-layers (bottom two layers constrained to bulk positions), with a 1×2 supercell repeat. The pristine slab totals 48 atoms, with 4 Ti and 8 O per tri-layer. 6 Å of vacuum are added on

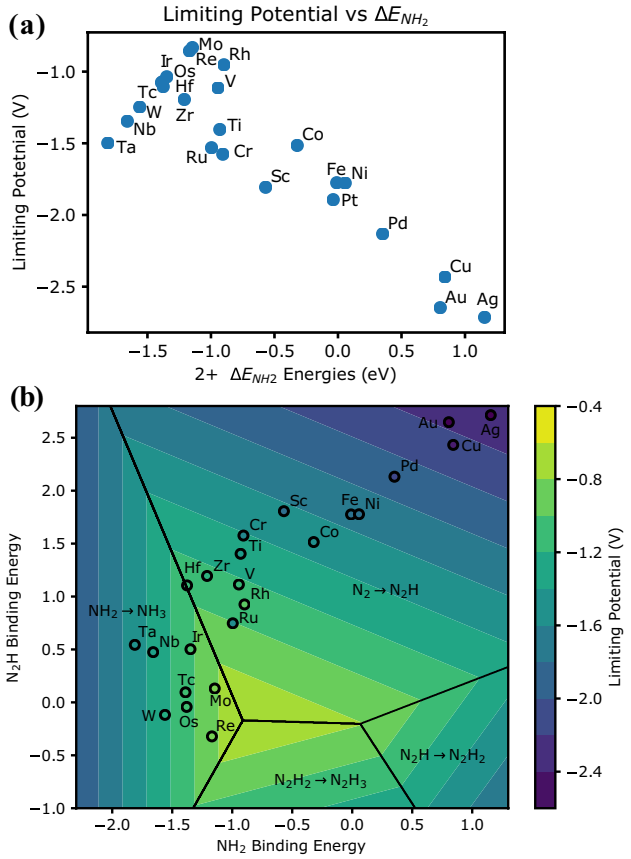

Fig. 6 **a** The limting potential vs the NH_2 binding energy. The data for this plot can be seen in Table S3. **b** A two dimensional volcano plot for electrochemical limiting potential using N_2H and NH_2 as descriptors for the studied systems. Points are colored in with the limiting potential calculated from DFT. Any surface for which a full path was not available has been excluded

both top and bottom of the slab and a dipole corrections is applied in the z direction [88]. The lattice parameters of the unit cells are fixed at the calculated value for pure rutile TiO_2. 2+ sites were created by replacing the six-fold titanium site with the substituent metal and removing a single bridging oxygen (see Fig. 1) 4+ sites were generated by replacing the five-fold titanium site with the substituent metal. The adsorption site was selected to directly over the substituent metals.

4.5 Adsorption Structure Optimization

To obtain reasonable initial guesses for structural optimization, all calculations were first performed using using Fe as the dopant metal. In these initial runs multiple adsorbate geometries were used as initial guesses. These converged structures were then used as initial guesses for all other dopant metals by replacing Fe with the corresponding metal. These structures were then allowed to relax to obtain the new lowest energy structure. All structures may be obtained from the provided SI.

Acknowledgements We would like to thank Fuhzu Liu and Gabriel Gusm˜ao for their comments and suggestions for improving this manuscript. This material is based upon work supported by the U. S. Department of Energy, Office of Science, Office of Basic Energy Sciences Computational Chemical Sciences program under Award No. DE-SC0019410.

References

1. Ritter SK (2018) The haber-bosch reaction: an early chemical impact on sustainability. Chem Eng News 86:1
2. Schlögl R (2003) Catalytic synthesis of ammonia—a "never-ending story"? Angew Chem Int Ed 42(18):2004–2008. https://doi.org/10.1002/anie.200301553
3. Smil V (1999) Detonator of the population explosion. Nature 400(6743):415–415. https://doi.org/10.1038/22672
4. Comer BM, Fuentes P, Dimkpa CO, Liu YH, Fernandez CA, Arora P, Realff M, Singh U, Hatzell MC, Medford AJ (2019) Prospects and challenges for solar fertilizers. Joule 3(7):1578–1605. https://doi.org/10.1016/j.joule.2019.05.001
5. Gross M (2012) We need to talk about nitrogen. Curr Biol. https://doi.org/10.1016/j.cub.2011.12.033
6. Schiffer ZJ, Manthiram K (2017) Electrification and decarbonization of the chemical industry. Joule 1(1):10–14. https://doi.org/10.1016/j.joule.2017.07.008
7. McPherson IJ, Sudmeier T, Fellowes J, Tsang SCE (2019) Materials for electrochemical ammonia synthesis. Dalton Trans 48(5):1562–1568. https://doi.org/10.1039/c8dt04019b
8. Wang L, Xia M, Wang H, Huang K, Qian C, Maravelias CT, Ozin GA (2018) Greening ammonia toward the solar ammonia refinery. Joule 2(6):1055–1074. https://doi.org/10.1016/j.joule.2018.04.017
9. Kyriakou V, Garagounis I, Vasileiou E, Vourros A, Stoukides M (2017) Progress in the electrochemical synthesis of ammonia. Catal Today 286:2–13. https://doi.org/10.1016/j.cattod.2016.06.014
10. de Bruijn FJ (2015) The quest for biological nitrogen fixation in cereals: a perspective and prospective. Biological nitrogen fixation. Wiley, Hoboken, pp 1087–1101. https://doi.org/10.1002/9781119053095.ch108
11. Michalsky R, Avram AM, Peterson BA, Pfromm PH, Peterson AA (2015) Chemical looping of metal nitride catalysts: low-pressure ammonia synthesis for energy storage. Chem Sci 6:3965–3974. https://doi.org/10.1039/C5SC00789E
12. Medford AJ, Hatzell MC (2017) Photon-driven nitrogen fixation: current progress, thermodynamic considerations, and future outlook. ACS Catal. https://doi.org/10.1021/acscatal.7b00439
13. Davies JA, Boucher DL, Edwards JG (1995) The question of artificial photosynthesis of ammonia on heterogeneous catalysts. Advances in photochemistry. Wiley, Hoboken, pp 235–310. https://doi.org/10.1002/9780470133507.ch4
14. Dhar N, Seshacharyulu E, Biswas N (1941) New aspects of nitrogen fixation and loss in soils. Proc Natl Inst Sci India 7:115–131
15. Schrauzer G, Guth T (1977) Photocatalytic reactions. 1. Photolysis of water and photoreduction of nitrogen on titanium dioxide. J Am Chem Soc 99(22):7189–7193
16. Schrauzer GN, Strampach N, Hui LN, Palmer MR, Salehi J (1983) Nitrogen photoreduction on desert sands under sterile conditions. Proc Natl Acad Sci USA 80(12):3873–3876

17. Bickley RI, Vishwanathan V (1979) Photocatalytically induced fixation of molecular nitrogen by near UV radiation. Nature 280(5720):306–308. https://doi.org/10.1038/280306a0
18. Augugliaro V, Lauricella A, Rizzuti L, Schiavello M, Sclafani A (1982) Conversion of solar energy to chemical energy by photoassisted processes—I. Preliminary results on ammonia production over doped titanium dioxide catalysts in a fluidized bed reactor. Int J Hydrog Energy 7(11):845–849. https://doi.org/10.1016/0360-3199(82)90001-5
19. Soria J, Conesa JC, Augugliaro V, Palmisano L, Schiavello M, Sclafani A (1991) Dinitrogen photoreduction to ammonia over titanium dioxide powders doped with ferric ions. J Phys Chem 95(1):274–282. https://doi.org/10.1021/j100154a052
20. Li C, Wang T, Zhao ZJ, Yang W, Li JF, Li A, Yang Z, Ozin GA, Gong J (2018) Promoted fixation of molecular nitrogen with surface oxygen vacancies on plasmon-enhanced TiO_2 photoelectrodes. Angew Chem Int Ed 57(19):5278–5282. https://doi.org/10.1002/anie.201713229
21. Yuan SJ, Chen JJ, Lin ZQ, Li WW, Sheng GP, Yu HQ (2013) Nitrate formation from atmospheric nitrogen and oxygen photocatalysed by nano-sized titanium dioxide. Nat Commun 4:1–7
22. Hirakawa H, Hashimoto M, Shiraishi Y, Hirai T (2017) Photocatalytic conversion of nitrogen to ammonia with water on surface oxygen vacancies of titanium dioxide. J Am Chem Soc 139(31):10929–10936. https://doi.org/10.1021/jacs.7b06634
23. Edwards JG, Davies JA, Boucher DL, Mennad A (1992) An opinion on the heterogeneous photoreactions of N_2 with H_2O. Angew Chem Int Ed 31(4):480–482
24. Davies JA, Edwards JG (1993) Reply: standards of demonstration for the heterogeneous photoreactions of N_2 with H_2O. Angew Chem Int Ed 32(4):552–553
25. Gao X, Wen Y, Qu D, An L, Luan S, Jiang W, Zong X, Liu X, Sun Z (2018) Interference effect of alcohol on Nessler's reagent in photocatalytic nitrogen fixation. ACS Sustain Chem Eng 6(4):5342–5348. https://doi.org/10.1021/acssuschemeng.8b00110
26. Cui X, Tang C, Zhang Q (2018) A review of electrocatalytic reduction of dinitrogen to ammonia under ambient conditions. Adv Energy Mater 8(22):1–25. https://doi.org/10.1002/aenm.201800369
27. Comer BM, Liu YH, Dixit MB, Hatzell KB, Ye Y, Crumlin EJ, Hatzell MC, Medford AJ (2018) The role of adventitious carbon in photo-catalytic nitrogen fixation by titania. J Am Chem Soc 140(45):15157–15160. https://doi.org/10.1021/jacs.8b08464
28. Zaleska A (2008) Doped-TiO_2: a review. Recent Pat Eng 2(3):157–164. https://doi.org/10.2174/187221208786306289
29. Schneider J, Matsuoka M, Takeuchi M, Zhang J, Horiuchi Y, Anpo M, Bahnemann DW (2014) Understanding TiO_2 photocatalysis: mechanisms and materials. Chem Rev 114(19):9919–9986. https://doi.org/10.1021/cr5001892
30. Li Y, Peng S, Jiang F, Lu G, Li S (2007) Effect of doping TiO_2 with alkaline-earth metal ions on its photocatalytic activity. J Serb Chem Soc 72(4):393–402. https://doi.org/10.2298/jsc0704393l
31. Dozzi MV, Selli E (2013) Doping TiO_2 with p- block elements: Effects on photocatalytic activity. J Photochem Photobiol C 14:13–28. https://doi.org/10.1016/j.jphotochemrev.2012.09.002
32. Ranjit K, Varadarajan T, Viswanathan B (1996) Photocatalytic reduction of dinitrogen to ammonia over noble-metal-loaded TiO_2. J Photochem Photobiol A 96(1–3):181–185. https://doi.org/10.1016/1010-6030(95)04290-3
33. Ranjit K, Viswanathan B (1997) Photocatalytic reduction of nitrite and nitrate ions to ammonia on m/TiO_2 catalysts. J Photochem Photobiol A 108(1):73–78. https://doi.org/10.1016/s1010-6030(96)04505-4
34. Comer BM, Medford AJ (2018) Analysis of photocatalytic nitrogen fixation on rutile TiO_2 (110). ACS Sustain Chem Eng 6(4):4648–4660. https://doi.org/10.1021/acssuschemeng.7b03652
35. Khan ME, Khan MM, Cho MH (2018) Recent progress of metal–graphene nanostructures in photocatalysis. Nanoscale 10(20):9427–9440. https://doi.org/10.1039/c8nr03500h
36. Gu XK, Qiao B, Huang CQ, Ding WC, Sun K, Zhan E, Zhang T, Liu J, Li WX (2014) Supported single pt1/au1 atoms for methanol steam reforming. ACS Catal 4(11):3886–3890. https://doi.org/10.1021/cs500740u
37. Ammal SC, Heyden A (2016) Water-gas shift activity of atomically dispersed cationic platinum versus metallic platinum clusters on titania supports. ACS Catal 7(1):301–309. https://doi.org/10.1021/acscatal.6b02764
38. Gu XK, Huang CQ, Li WX (2017) Firstprinciples study of single transition metal atoms on ZnO for the water gas shift reaction. Catal Sci Technol 7(19):4294–4301. https://doi.org/10.1039/c7cy00704c
39. García-Mota M, Vojvodic A, Metiu H, Man IC, Su HY, Rossmeisl J, Nørskov JK (2011) Tailoring the activity for oxygen evolution electrocatalysis on rutile TiO_2 (110) by transition-metal substitution. ChemCatChem 3(10):1607–1611. https://doi.org/10.1002/cctc.201100160
40. Yao Z, Reuter K (2017) First-principles computational screening of dopants to improve the deacon process over RuO_2. ChemCatChem 10(2):465–469. https://doi.org/10.1002/cctc.201701313
41. Liu J (2016) Catalysis by supported single metal atoms. ACS Catal 7(1):34–59. https://doi.org/10.1021/acscatal.6b01534
42. Qiao B, Wang A, Yang X, Allard LF, Jiang Z, Cui Y, Liu J, Li J, Zhang T (2011) Single-atom catalysis of CO oxidation using pt1/FeOx. Nat Chem 3(8):634–641. https://doi.org/10.1038/nchem.1095
43. O'Connor NJ, Jonayat ASM, Janik MJ, Senftle TP (2018) Interaction trends between single metal atoms and oxide supports identified with density functional theory and statistical learning. Nat Catal 1(7):531–539. https://doi.org/10.1038/s41929-018-0094-5
44. Tao H, Choi C, Ding LX, Jiang Z, Han Z, Jia M, Fan Q, Gao Y, Wang H, Robertson AW, Hong S, Jung Y, Liu S, Sun Z (2019) Nitrogen fixation by ru single-atom electrocatalytic reduction. Chem 5(1):204–214. https://doi.org/10.1016/j.chempr.2018.10.007
45. Liu S, Wang Y, Wang S, You M, Hong S, Wu TS, Soo YL, Zhao Z, Jiang G, Qiu J, Wang B, Sun Z (2019) Photocatalytic fixation of nitrogen to ammonia by single Ru atom decorated TiO_2 nanosheets. ACS Sustain Chem Eng 7(7):6813–6820. https://doi.org/10.1021/acssuschemeng.8b06134
46. Zhao Z, Hong S, Yan C, Choi C, Jung Y, Liu Y, Liu S, Li X, Qiu J, Sun Z (2019) Efficient visible-light driven n_2 fixation over two-dimensional sb/TiO_2 composites. Chem Commun 55(50):7171–7174. https://doi.org/10.1039/c9cc02291k
47. Cheng S, Gao YJ, Yan YL, Gao X, Zhang SH, Zhuang GL, Deng SW, Wei ZZ, Zhong X, Wang JG (2019) Oxygen vacancy enhancing mechanism of nitrogen reduction reaction property in Ru/TiO_2. J Energy Chem 39:144–151. https://doi.org/10.1016/j.jechem.2019.01.020
48. Li SJ, Bao D, Shi MM, Wulan BR, Yan JM, Jiang Q (2017) Amorphizing of au nanoparticles by CeOx-RGO hybrid support towards highly efficient electrocatalyst for n2reduction under ambient conditions. Adv Mater 29(33):1700001. https://doi.org/10.1002/adma.201700001
49. Diebold U (2003) The surface science of titanium dioxide. Surf Sci Rep 48(5–8):53–229. https://doi.org/10.1016/s0167-5729(02)00100-0
50. Yates JT Jr, Szabó A, Henderson MA (1991) The influence of surface defect sites on chemisorption and catalysis. Structure-activity

and selectivity relationships in heterogeneous catalysis, proceedings of the ACS symposium on structure-activity relationships in heterogeneous catalysis. Elsevier, Amsterdam, pp 273–290. https://doi.org/10.1016/s0167-2991(08)61945-x
51. Lu G, Linsebigler A, Yates JT (1994) Ti^{3+} defect sites on TiO_2 (110): production and chemical detection of active sites. J Phys Chem 98(45):11733–11738. https://doi.org/10.1021/j100096a017
52. Walle LE, Borg A, Uvdal P, Sandell A (2009) Experimental evidence for mixed dissociative and molecular adsorption of water on a rutile TiO_2 (110) surface without oxygen vacancies. Phys Rev B 80(23):235436. https://doi.org/10.1103/PhysRevB.80.235436
53. García-Mota M, Vojvodic A, Abild-Pedersen F, Nørskov JK (2012) Electronic origin of the surface reactivity of transition-metal-doped TiO_2 (110). J Phys Chem C 117(1):460–465. https://doi.org/10.1021/jp310667r
54. Höskuldsson AB, Abghoui Y, Gunnarsdóttir AB, Skúlason E (2017) Computational screening of rutile oxides for electrochemical ammonia formation. ACS Sustain Chem Eng 5(11):10327–10333. https://doi.org/10.1021/acssuschemeng.7b02379
55. Montoya JH, Tsai C, Vojvodic A, Nørskov JK (2015) The challenge of electrochemical ammonia synthesis: a new perspective on the role of nitrogen scaling relations. Chemsuschem 8(13):2180–2186
56. Ruban A, Hammer B, Stoltze P, Skriver H, Nørskov J (1997) Surface electronic structure and reactivity of transition and noble metals. J Mol Catal A 115(3):421–429. https://doi.org/10.1016/s1381-1169(96)00348-2
57. Hammer B, Nørskov J (2000) Theoretical surface science and catalysis—calculations and concepts. Advances in catalysis. Elsevier, Amsterdam, pp 71–129. https://doi.org/10.1016/s0360-0564(02)45013-4
58. Xu Z, Kitchin JR (2015) Relationships between the surface electronic and chemical properties of doped 4d and 5d late transition metal dioxides. J Chem Phys 142(10):104703. https://doi.org/10.1063/1.4914093
59. Iliev V, Tomova D, Bilyarska L, Eliyas A, Petrov L (2006) Photocatalytic properties of TiO_2 modified with platinum and silver nanoparticles in the degradation of oxalic acid in aqueous solution. Appl Catal B 63(3–4):266–271. https://doi.org/10.1016/j.apcatb.2005.10.014
60. Dang TMD, Nguyen TMH, Nguyen HP (2010) The preparation of nano-gold catalyst supported on iron doped titanium oxide. Adv Nat Sci 1(2):025011. https://doi.org/10.1088/2043-6254/1/2/025011
61. Shinde VM, Madras G (2013) CO methanation toward the production of synthetic natural gas over highly active Ni/TiO_2 catalyst. AIChE J 60(3):1027–1035. https://doi.org/10.1002/aic.14304
62. Yu J, Yu J, Shi Z, Guo Q, Xiao X, Mao H, Mao D (2019) The effects of the nature of TiO_2 supports on the catalytic performance of Rh–Mn/TiO_2 catalysts in the synthesis of C_2 oxygenates from syngas. Catal Sci Technol 9(14):3675–3685. https://doi.org/10.1039/c9cy00406h
63. Bagheri S, Julkapli NM, Hamid SBA (2014) Titanium dioxide as a catalyst support in heterogeneous catalysis. Sci World J 2014:1–21. https://doi.org/10.1155/2014/727496
64. Nilsson A, Pettersson LG (2008) Adsorbate electronic structure and bonding on metal surfaces. Chemical bonding at surfaces and interfaces. Elsevier, Amsterdam, pp 57–142. https://doi.org/10.1016/b978-044452837-7.50003-4
65. Mizutani U, Inukai M, Sato H, Zijlstra E (2014) 2 Electron theory of complex metallic alloys. In: Laughlin DE, Hono K (eds) Physical metallurgy, 5th edn. Elsevier, Oxford, pp 103–202. https://doi.org/10.1016/B978-0-444-53770-6.00002-2
66. Hammer B, Norskov JK (1995) Why gold is the noblest of all the metals. Nature 376(6537):238–240. https://doi.org/10.1038/376238a0
67. Gani TZH, Kulik HJ (2018) Understanding and breaking scaling relations in single-site catalysis: methane to methanol conversion by Fe^{IV} =O. ACS Catal 8(2):975–986. https://doi.org/10.1021/acscatal.7b03597
68. Darby MT, Stamatakis M, Michaelides A, Sykes ECH (2018) Lonely atoms with special gifts: breaking linear scaling relationships in heterogeneous catalysis with single-atom alloys. J Phys Chem Lett 9(18):5636–5646. https://doi.org/10.1021/acs.jpclett.8b01888
69. Turchanin MA, Agraval PG (2008) Cohesive energy, properties, and formation energy of transition metal alloys. Powder Metall Metal Ceram 47(1–2):26–39. https://doi.org/10.1007/s11106-008-0006-3
70. Nørskov JK, Rossmeisl J, Logadottir A, Lindqvist L, Kitchin JR, Bligaard T, Jonsson H, (2004) Origin of the overpotential for oxygen reduction at a fuel-cell cathode. J Phys Chem B 108(46):17886–17892. https://doi.org/10.1021/jp047349j
71. Seh ZW, Kibsgaard J, Dickens CF, Chorkendorff I, Nørskov JK, Jaramillo TF (2017) Combining theory and experiment in electrocatalysis: Insights into materials design. Science. https://doi.org/10.1126/science.aad4998
72. Wang S, Petzold V, Tripkovic V, Kleis J, Howalt JG, Skulason E, Fernandez EM, Hvolbæk B, Jones G, Toftelund A, Falsig H, Bjrketun M, Studt F, Abild-Pedersen F, Rossmeisl J, Nørskov JK, Bligaard T (2011) Universal transition state scaling relations for (de)hydrogenation over transition metals. Phys Chem Chem Phys 13(46):20760. https://doi.org/10.1039/c1cp20547a
73. Nozik AJ, Memming R (1996) Physical chemistry of semiconductor-liquid interfaces. J Phys Chem 100(31):13061–13078. https://doi.org/10.1021/jp953720e
74. Vesborg PCK, Jaramillo TF (2012) Addressing the terawatt challenge: scalability in the supply of chemical elements for renewable energy. RSC Adv 2(21):7933. https://doi.org/10.1039/c2ra20839c
75. Hernandez JA, George SJ, Rubio LM (2009) Molybdenum trafficking for nitrogen fixation. Biochemistry 48(41):9711–9721. https://doi.org/10.1021/bi901217p
76. Roux Y, Duboc C, Gennari M (2017) Molecular catalysts for n 2 reduction: state of the art, mechanism, and challenges. ChemPhysChem 18(19):2606–2617. https://doi.org/10.1002/cphc.201700665
77. Greenlee LF, Renner JN, Foster SL (2018) The use of controls for consistent and accurate measurements of electrocatalytic ammonia synthesis from dinitrogen. ACS Catal 8(9):7820–7827. https://doi.org/10.1021/acscatal.8b02120
78. Andersen SZ, Čolić V, Yang S, Schwalbe JA, Nielander AC, McEnaney JM, Enemark-Rasmussen K, Baker JG, Singh AR, Rohr BA, Statt MJ, Blair SJ, Mezzavilla S, Kibsgaard J, Ves-borg PCK, Cargnello M, Bent SF, Jaramillo TF, Stephens IEL, Nørskov JK, Chorkendorff I (2019) A rigorous electrochemical ammonia synthesis protocol with quantitative isotope measurements. Nature 570(7762):504–508. https://doi.org/10.1038/s41586-019-1260-x
79. Giannozzi P, Baroni S, Bonini N, Calandra M, Car R, Cavazzoni C, Ceresoli D, Chiarotti GL, Cococcioni M, Dabo I, Dal Corso A, de Gironcoli S, Fabris S, Fratesi G, Gebauer R, Gerstmann U, Gougoussis C, Kokalj A, Lazzeri M, Martin-Samos L, Marzari N, Mauri F, Mazzarello R, Paolini S, Pasquarello A, Paulatto L, Sbraccia C, Scandolo S, Sclauzero G, Seitsonen AP, Smogunov A, Umari P, Wentzcovitch RM (2009) Quantum espresso: a modular and open-source software project for quantum simulations of materials. J Phys 21(39):395502
80. Larsen AH, Mortensen JJ, Blomqvist J, Castelli IE, Christensen R, Duak M, Friis J, Groves MN, Hammer B, Hargus C, Hermes ED, Jennings PC, Jensen PB, Kermode J, Kitchin JR, Kolsbjerg

EL, Kubal J, Kaasbjerg K, Lysgaard S, Maronsson JB, Maxson T, Olsen T, Pastewka L, Peterson A, Rostgaard C, Schitz J, Schtt O, Strange M, Thygesen KS, Vegge T, Vilhelmsen L, Walter M, Zeng Z, Jacobsen KW (2017) The atomic simulation environmenta python library for working with atoms. J Phys 29(27):273002

81. Wellendorff J, Lundgaard KT, Møgelhøj A, Petzold V, Landis DD, Nørskov JK, Bligaard T, Jacobsen KW (2012) Density functionals for surface science: Exchange-correlation model development with bayesian error estimation. Phys Rev B 85(23):235149–235149. https://doi.org/10.1103/PhysRevB.85.235149
82. Monkhorst HJ, Pack JD (1976) Special points for brillouin-zone integrations. Phys Rev B 13(12):5188–5192. https://doi.org/10.1103/physrevb.13.5188
83. Prandini G, Marrazzo A, Castelli IE, Mounet N, Marzari N (2018) A standard solid state pseudopotentials (sssp) library optimized for accuracy and efficiency (version 1.0, data download). Mater Cloud Arch. https://doi.org/10.24435/materialscloud:2018.0001/v1
84. Lejaeghere K, Bihlmayer G, Björkman T, Blaha P, Blügel S, Blum V, Caliste D, Castelli IE, Clark SJ, Dal Corso A, De Gironcoli S, Deutsch T, Dewhurst JK, Di Marco I, Draxl C, Du Lak M, Eriksson O, Flores-Livas JA, Garrity KF, Genovese L, Giannozzi P, Giantomassi M, Goedecker S, Gonze X, Grånäs O, Gross EKU, Gulans A, Gygi F, Hamann DR, Hasnip PJ, Holzwarth NAW, Iuşan D, Jochym DB, Jollet F, Jones D, Kresse G, Koepernik K, Küçükbenli E, Kvashnin YO, Locht ILM, Lubeck S, Marsman M, Marzari N, Nitzsche U, Nordström L, Ozaki T, Paulatto L, Pickard CJ, Poelmans W, Probert MIJ, Refson K, Richter M, Rignanese GM, Saha S, Scheffler M, Schlipf M, Schwarz K, Sharma S, Tavazza F, Thunström P, Tkatchenko A, Torrent M, Vanderbilt D, van Setten MJ, Van Speybroeck V, Wills JM, Yates JR, Zhang GX, Cottenier S (2016) Reproducibility in density functional theory calculations of solids. Science. https://doi.org/10.1126/science.aad3000
85. Anisimov VI, Zaanen J, Andersen OK (1991) Band theory and mott insulators: Hubbard U instead of Stoner I. Phys Rev B 44(3):943–954. https://doi.org/10.1103/physrevb.44.943
86. Reuter K, Stampf C, Scheffler M (2005) AB initio atomistic thermodynamics and statistical mechanics of surface properties and functions. Handbook of materials modeling. Springer, Berlin, pp 149–194
87. Hellman A, Wang B (2017) First-principles view on photoelectrochemistry: water-splitting as case study. Inorganics 5(2):37. https://doi.org/10.3390/inorganics5020037
88. Bengtsson L (1999) Dipole correction for surface supercell calculations. Phys Rev B 59:12301–12304. https://doi.org/10.1103/PhysRevB.59.12301

Affiliations

Benjamin M. Comer[1] · Max H. Lenk[2] · Aradhya P. Rajanala[3] · Emma L. Flynn[4] · Andrew J. Medford[1]

✉ Andrew J. Medford
andrew.medford@chbe.gatech.edu

[1] School of Chemical and Biomolecular Engineering, Georgia Institute of Technology, 311 Ferst Drive NW, Atlanta, GA 30318, USA

[2] School of Materials Science and Engineering, Georgia Institute of Technology, Atlanta, USA

[3] School of Physics, Georgia Institute of Technology, Atlanta, USA

[4] School of Computer Science, Georgia Institute of Technology, Atlanta, USA